

University of Groningen

## Engineered Near-Infrared Fluorescent Protein Assemblies for Robust Bioimaging and Therapeutic Applications

Li, Jingjing; Li, Bo; Sun, Jing; Ma, Chao; Wan, Sikang; Li, Yuanxin; Goestl, Robert; Herrmann, Andreas; Liu, Kai; Zhang, Hongjie

*Published in:*  
Advanced materials

*DOI:*  
[10.1002/adma.202000964](https://doi.org/10.1002/adma.202000964)

**IMPORTANT NOTE: You are advised to consult the publisher's version (publisher's PDF) if you wish to cite from it. Please check the document version below.**

*Document Version*  
Publisher's PDF, also known as Version of record

*Publication date:*  
2020

[Link to publication in University of Groningen/UMCG research database](#)

*Citation for published version (APA):*

Li, J., Li, B., Sun, J., Ma, C., Wan, S., Li, Y., Goestl, R., Herrmann, A., Liu, K., & Zhang, H. (2020). Engineered Near-Infrared Fluorescent Protein Assemblies for Robust Bioimaging and Therapeutic Applications. *Advanced materials*, 32(17), [2000964]. <https://doi.org/10.1002/adma.202000964>

### Copyright

Other than for strictly personal use, it is not permitted to download or to forward/distribute the text or part of it without the consent of the author(s) and/or copyright holder(s), unless the work is under an open content license (like Creative Commons).

The publication may also be distributed here under the terms of Article 25fa of the Dutch Copyright Act, indicated by the "Taverne" license. More information can be found on the University of Groningen website: <https://www.rug.nl/library/open-access/self-archiving-pure/taverne-amendment>.

### Take-down policy

If you believe that this document breaches copyright please contact us providing details, and we will remove access to the work immediately and investigate your claim.

Downloaded from the University of Groningen/UMCG research database (Pure): <http://www.rug.nl/research/portal>. For technical reasons the number of authors shown on this cover page is limited to 10 maximum.

# Engineered Near-Infrared Fluorescent Protein Assemblies for Robust Bioimaging and Therapeutic Applications

Jingjing Li, Bo Li, Jing Sun, Chao Ma, Sikang Wan, Yuanxin Li, Robert Göstl, Andreas Herrmann, Kai Liu,\* and Hongjie Zhang

Fluorescent proteins are investigated extensively as markers for the imaging of cells and tissues that are treated by gene transfection. However, limited transfection efficiency and lack of targeting restrict the clinical application of this method rooted in the challenging development of robust fluorescent proteins for in vivo bioimaging. To address this, a new type of near-infrared (NIR) fluorescent protein assemblies manufactured by genetic engineering is presented. Due to the formation of well-defined nanoparticles and spectral operation within the phototherapeutic window, the NIR protein aggregates allow stable and specific tumor imaging via simple exogenous injection. Importantly, in vivo tumor metastases are tracked and this overcomes the limitations of in vivo imaging that can only be implemented relying on the gene transfection of fluorescent proteins. Concomitantly, the efficient loading of hydrophobic drugs into the protein nanoparticles is demonstrated facilitating the therapy of tumors in a mouse model. It is believed that these theranostic NIR fluorescent protein assemblies, hence, show great potential for the in vivo detection and therapy of cancer.

(700–1700 nm) offers increased tissue penetration depths and a better signal-to-noise ratio rendering it ideal for biomedical applications.<sup>[1–7]</sup> Currently, NIR fluorescent materials mainly comprise quantum dots,<sup>[8–10]</sup> lanthanide-doped upconverting nanoparticles,<sup>[11–13]</sup> organic small molecules,<sup>[14,15]</sup> and polymer-based systems.<sup>[16]</sup> However, long-term toxicity and immunogenicity, non-biodegradability, as well as photo-instability of these non-life-like materials have restricted their translation into clinical applications.<sup>[17–22]</sup> Thus, the development of new fluorophores with increased biocompatibility and biosafety as imaging diagnostic tools is essential for biomedical application.

Fluorescent proteins (FPs), such as red-shifted fluorescent protein and engineered monomeric near-infrared fluorescent proteins (mIFPs), were proven to be excellent candidates for noninvasive labeling and

Near-infrared (NIR) fluorescence imaging is an evolving field enabling high-resolution imaging and diagnosis in biomedicine. Due to the reduced photon scattering and minimal tissue absorption, fluorescence imaging in the NIR window

whole-body imaging in living organisms due to the low light scattering/background noise, reduced autofluorescence, and relatively easy construction procedure.<sup>[23–30]</sup> Typically, those fluorophores are genetically encoded and must be produced by gene transfection into living cells and animals for bioimaging. However, the transfection efficiency is limited and the FPs expressed by this procedure are unable to target tumors effectively owing to the lack of specific binding sites.<sup>[31,32]</sup> Moreover, FPs that are expressed by hosts such as *Escherichia coli* and yeast are rarely reported for direct in vivo bioimaging. This most likely stems from the fast photobleaching in blood proteases environment when the FPs are injected exogenously. Therefore, it remains a major challenge to develop robust FPs for the realization of stable and specific bioimaging and diagnosis via a simple and direct exogenous injection of the fluorescent markers.

Here, we demonstrate a new type of well-defined mIFP nanoassembly, which is driven by electrostatic complexation of positively charged mIFP conjugates and anionic carboxylate-terminated poly(ethylene glycol) (PEG-COO<sup>-</sup>) chains. The resulting protein nanoparticles exhibit outstanding NIR emission and photostability, high cell permeability, good biocompatibility, and significantly improved blood circulation time. Stable and long-time imaging characteristics at the tumor sites were achieved through a single intravenous injection, which is far superior to other FPs reported to date. Interestingly, the mIFP assemblies were accumulated effectively in the metastatic


Dr. J. Li, B. Li, Dr. J. Sun, S. Wan, Y. Li, Prof. K. Liu, Prof. H. Zhang  
State Key Laboratory of Rare Earth Resource Utilization  
Changchun Institute of Applied Chemistry  
Chinese Academy of Sciences  
Changchun 130022, China  
E-mail: kai.liu@ciac.ac.cn

Dr. J. Sun, Dr. C. Ma, Prof. A. Herrmann  
Zernike Institute for Advanced Materials  
University of Groningen  
Nijenborgh 4, Groningen 9747 AG, The Netherlands

Dr. R. Göstl, Prof. A. Herrmann  
DWI–Leibniz Institute for Interactive Materials  
Forckenbeckstr. 50, Aachen 52056, Germany

Prof. A. Herrmann  
Institute of Technical and Macromolecular Chemistry  
RWTH Aachen University  
Worringerweg 1, Aachen 52074, Germany

Prof. K. Liu, Prof. H. Zhang  
Department of Chemistry  
Tsinghua University  
Beijing 100084, China

 The ORCID identification number(s) for the author(s) of this article can be found under <https://doi.org/10.1002/adma.202000964>.

DOI: 10.1002/adma.202000964

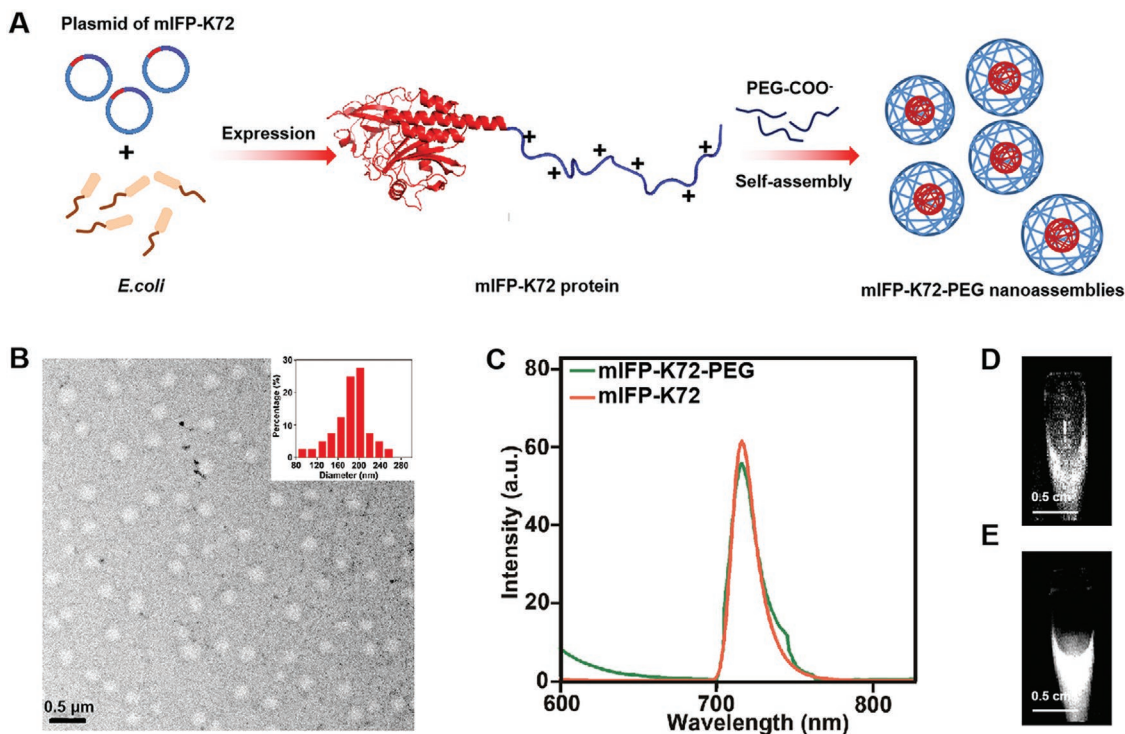


**Figure 1.** The synthesis and characterization of mIFP-K72-PEG nanoassemblies. A) Schematic representation for the fabrication of mIFP-K72-PEG assemblies. The protein mIFP-K72 was genetically fused with a cationic polypeptide of (VPGKG)<sub>72</sub> to the C-terminus of mIFP by recombinant DNA technology and expressed in *Escherichia coli*. By complexation with negatively charged PEG-COO<sup>-</sup>, the mIFP-K72-PEG protein assemblies were produced. B) TEM image and size distribution of the mIFP-K72-PEG. The protein assemblies exhibit a uniform spherical structure with an average size of about 200 nm in diameter. Scale bar: 0.5  $\mu$ m. C) Emission spectra of mIFP-K72 and mIFP-K72-PEG ( $\lambda_{\text{ex}} = 680$  nm). Images of the fluorescent mIFP-K72-PEG complex ( $16 \times 10^{-6}$  M) in D) blood and E) PBS buffer. Here  $\lambda_{\text{ex}} = 665$  nm and  $\lambda_{\text{em}} = 710$  nm.

tumor nodules in mice liver, confirming their passive specific targeting capability. Furthermore, it was found that the hydrophobic antitumor antibiotic of thiostrepton was efficiently encapsulated within the protein nanoaggregates and effective tumor therapy in mice model was realized. Therefore, the development of mIFP-based assemblies offers new opportunities to explore bioimaging and quasi-segment therapeutic applications in clinical trials.

The protein nanoparticle assembly is a two-component system, including a cationic chimera protein and a chemically synthesized anionic polyelectrolyte (Figure 1A). The protein entity consists of recombinant mIFP or GFP and cationic fusion polypeptides. This highly charged species is derived from elastin-like pentapeptide (ELP) with characteristic repeat units (VPGKG)<sub>n</sub>. Notably, the digit here denotes the amounts of charges involved in the specific recombinant protein. A series of chimera samples, including mIFP-K72 and GFP-K72, and other polypeptides, including K18 and K36 for control experiments, were designed and prepared (preparation details are given in Supporting Information, Figures S1 and S2 and Table S1, Supporting Information).<sup>[33,34]</sup> All proteins were characterized by both polyacrylamide gel electrophoresis and matrix-assisted laser desorption/ionization time-of-flight mass spectrometry, respectively (Figures S3 and S4, Supporting Information). The anionic polyelectrolyte component is a biocompatible carboxylated polyethylene glycol (PEG-COO<sup>-</sup>) (Figure S5, Supporting Information). PEGylation was performed through combination

of anionic PEG-COO<sup>-</sup> and cationic mIFP-K72 conjugates by electrostatic interaction, generating mIFP-based nanoparticles (e.g., mIFP-K72-PEG).

The morphology of the assembled protein nanostructures was investigated using transmission electron microscopy (TEM) and atomic force microscopy. As shown in Figure 1B and Figure S6, Supporting Information, a highly uniform spherical structure of mIFP-K72-PEG with an average size of about 200 nm in diameter was observed. This was consistent with dynamic light scattering analysis, in which the hydrodynamic size of the prepared protein assemblies was determined to be  $\approx 200$  nm (Figure S7, Supporting Information). In the protein-PEG complex, the hydrophobic properties of the mIFP chromophore and its charge shielded elastin-like chains together with the hydrophilic PEG chains endowed mIFP-K72-PEG with amphiphilic characteristics, resulting in the aggregation and phase separation in aqueous solutions and thereby formed nanoparticles. As the neutralization of positively charged ELP polypeptide, the typical behavior with phase transition from soluble to insoluble state might also contribute to the nanoparticle formation. Moreover, the nanoaggregation behaviors of the K36-PEG and K18-PEG were investigated, indicating that the nanoparticle sizes can be manipulated by the length of the fused K polypeptides (Figures S7–S9, Supporting Information). Next, the fluorescence spectra of the complexed mIFP-K72-PEG and the pristine mIFP-K72 were recorded (Figure 1C). It was found that both showed comparable emission peaks

around 710 nm, suggesting that the PEGylation on mIFP-K72 had negligible effect on its intrinsic structure and fluorescence performance. In addition, there was no significant fluorescence alteration for the mIFP-K72-PEG within 1 week, highlighting the photostability of the protein assemblies in blood serum (Figure S10, Supporting Information).

The cytotoxicity of the mIFP-K72-PEG nanoparticles was investigated by propidium iodide and calcein AM staining assays in human fibroblast cells. As shown in Figure S11, Supporting Information, the cell viability remained at 95% after 24 h incubation with  $800 \times 10^{-6}$  M of the protein sample. Moreover, the *in vivo* toxicity was assessed by intravenous injection of the mIFP-K72-PEG in a mouse model (Animal experiments were approved by the Institutional Animal Care and Use Committee of Jilin University). Over a period of 2 weeks, a survival rate of 100% was observed and no difference in the mice' overall appearance when treated with the protein sample and phosphate-buffered saline (PBS), respectively, could be noted (Figure S12, Supporting Information). Furthermore, the cellular uptake of the protein assemblies in HeLa cells was investigated. Since the bathochromic excitation wavelength ( $\lambda_{\text{ex}} = 680$  nm) of the mIFP-K72-PEG was not available in our applied fluorescence microscopy setup, here the GFP-K72-PEG

as an alternative was utilized. Intracellular fluorescence of HeLa cells treated with the GFP-K72-PEG sample was observed when incubated for 10 min (Figure S13, Supporting Information), confirming the efficient cellular uptake of the protein nanoparticles.

Fluorescent nanoparticles typically target tumors via passive accumulation due to the enhanced permeability and retention (EPR) effect.<sup>[35,36]</sup> A comparably large size is useful to prevent penetration of nanoparticles into normal cells and increase accumulation in the target tissue and thus enhance signal intensity within the target. In the present system, K72-PEG was larger compared to K36-PEG and K18-PEG (Figure S9, Supporting Information). Thus, the feasibility of the mIFP-K72-PEG probe for *in vivo* tumor imaging was investigated. For this purpose, a tumor xenograft was induced in the right hind leg of mice by subcutaneous injection of HeLa cells. After inoculation for 3 weeks, the mice were intravenously injected with the mIFP-K72-PEG ( $800 \text{ nmol kg}^{-1}$ ), GFP-K72-PEG ( $800 \text{ nmol kg}^{-1}$ ), and PBS buffer, respectively. Fluorescence imaging was performed using a Maestro (CRi) *in vivo* imaging system and analyzed at multiple time points after injection (Figure 2). No fluorescence was detected in mice when treated with GFP-K72-PEG, suggesting photoinstability and poor

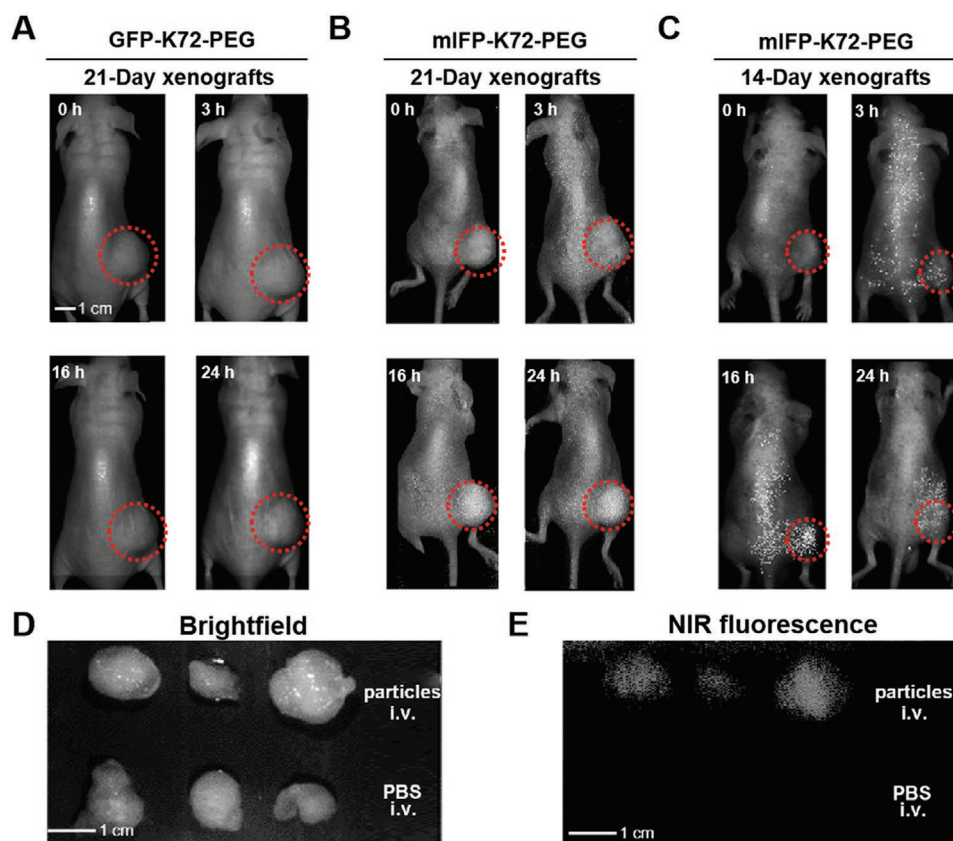


**Figure 2.** *In vivo* and *ex vivo* imaging of tumor xenografts. Tumor xenograft was induced in the right hind leg of mice by subcutaneous injection of HeLa cells. HeLa cells were incubated for A,B) 3 or C) 2 weeks, respectively. A,B) *In vivo* NIR fluorescence imaging of mice with tumor xenografts in the right hind leg after administration of GFP-K72-PEG (A,  $800 \text{ nmol kg}^{-1}$ ) or mIFP-K72-PEG (B,  $800 \text{ nmol kg}^{-1}$ ). C) *In vivo* NIR fluorescence imaging for earlier detection of tumor xenografts after injection of mIFP-K72-PEG ( $800 \text{ nmol kg}^{-1}$ ). D,E) Brightfield and NIR fluorescence imaging of excised tumor xenografts. *Ex vivo* imaging analysis was performed by harvesting tumor xenografts from mice treated with mIFP-K72-PEG (upper panel) or PBS (lower panel) at 24 h post-injection ( $N = 3$ ). Tumor sites are indicated by dashed circles. Scale bar: 1 cm. NIR fluorescence imaging:  $\lambda_{\text{ex}} = 665$  nm and  $\lambda_{\text{em}} = 710$  nm.



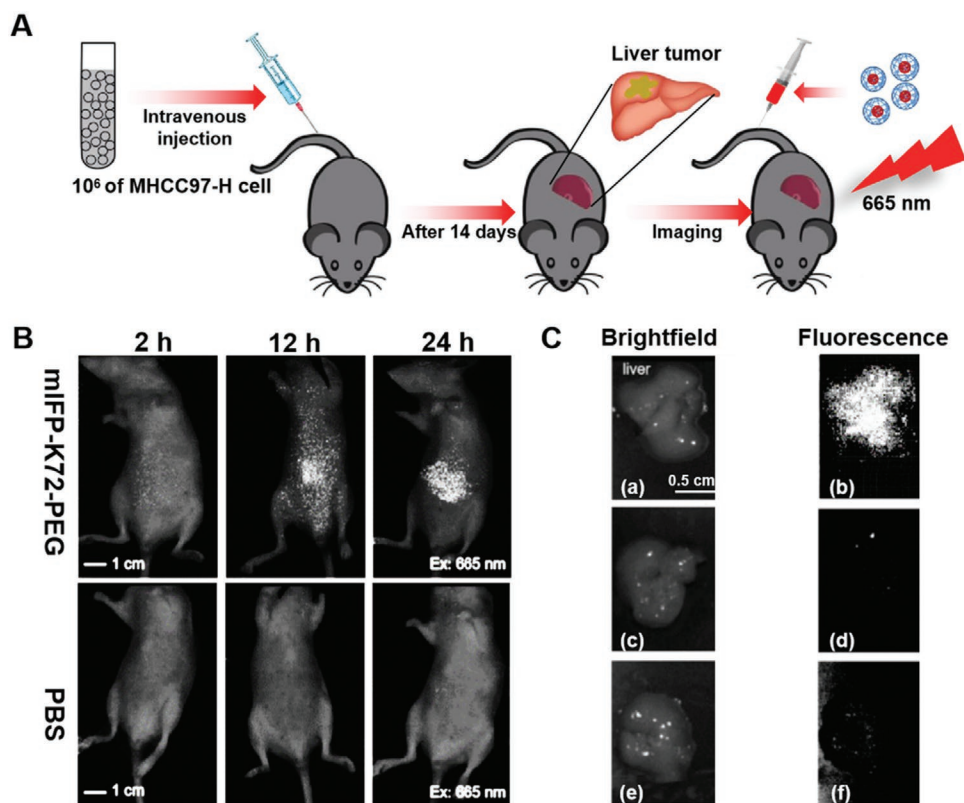


**Figure 3.** In vivo and ex vivo imaging of metastatic tumor nodules. A) Schematic representation for imaging mice metastatic tumor nodules. The human hepatocellular carcinoma cells (MHCC97-H) were inoculated intravenously and incubated for 2 weeks in mice, followed by intravenous injection of the mIFP-K72-PEG protein nanoparticles. The images were recorded after irradiation with light at  $\lambda_{\text{ex}} = 665 \text{ nm}$ . B) In vivo NIR fluorescence imaging of mice with metastatic tumor nodules in liver after administration of mIFP-K72-PEG ( $800 \text{ nmol kg}^{-1}$ ). PBS-treated as a control group. Scale bar: 1 cm. C) Ex vivo imaging of mice tissues from different groups: the mice injected with a,b) both MHCC97-H cells and mIFP-K72-PEG, c,d) mice treatment only with mIFP-K72-PEG or e,f) PBS buffer. Only the group treated with both MHCC97-H cells and mIFP-K72-PEG exhibited the fluorescent signals in the liver. Scale bar: 0.5 cm. NIR fluorescence imaging:  $\lambda_{\text{ex}} = 665 \text{ nm}$  and  $\lambda_{\text{em}} = 710 \text{ nm}$ .

penetration depth of the GFP derivatives for in vivo bioimaging (Figure 2A; Figure S14, Supporting Information).<sup>[37]</sup> Most notably, however, the fluorescence emitted from the mIFP-K72-PEG assemblies was easily recorded on the tumor sites at 16 h post-injection and the fluorescence maintained well even after 24 h (Figures 2B). The fluorescence signal gradually faded after 36 h, which might be ascribed to the clearance and degradation of the protein assemblies in the tumor surrounding proteases environment. It should be noted that the 36 h imaging characteristic of the NIR protein nanoparticles is sufficient for diagnostic test in future clinical applications. Furthermore, the size effect of tumor xenograft on the in vivo imaging was explored by shortening the inoculation time with HeLa cells to 2 weeks. Immediately after tail vein injection, the fluorescent marker was extensively distributed throughout the entire mice at 3 h post-injection (Figure 2C). It was found that fluorescence intensities at the tumor site were increased at 16 and 24 h post-injection, suggesting the mIFP-K72-PEG nanoassemblies gradually permeated tumors through passive targeting and EPR effect. Those experiments confirmed the capacity of mIFP-K72-PEG for tumors' imaging and diagnostics even though at early stage, they are in small sizes. Ex vivo imaging analysis was performed by harvesting tumor xenografts from the right hind legs of mice at 24 h post-injection (Figure 2D,E). In comparison

with the PBS control group, the tumor xenografts treated by the mIFP-K72-PEG exhibited obvious fluorescence. These results demonstrate that the mIFP-K72-PEG accumulated in tumor sites specifically, indicating mIFP-based assemblies are applicable for in vivo tumor imaging. Moreover, in the present system, the PEGylation with the proteins might be important to prevent early recognition of the nanoparticles by the immune system,<sup>[38]</sup> thus leading to increased circulation time of protein assemblies in blood and enhance their stability in vivo.

Due to the robust in vivo fluorescence imaging of mIFP-K72-PEG, we next investigated our protein assemblies as fluorescent probes for the detection of metastatic tumor nodules. This was carried out using a mice cancer model of liver metastasis. As depicted in Figure 3A,  $\approx 10^6$  of human hepatocellular carcinoma cells (MHCC97-H) were inoculated intravenously and incubated for 2 weeks in mice, followed by intravenous injection of the mIFP-K72-PEG nanoparticles (Figure 3A). Significant fluorescence around the liver was achieved at 12 h post-injection of the protein sample when comparing with the PBS treatment (Figure 3B). In addition, it was found that the fluorescence signal in the liver area gradually increased after 12 and 24 h post-injection, respectively. An outstanding fluorescence contrast between the tumor and normal tissues was observed, clearly confirming a high uptake and accumulation

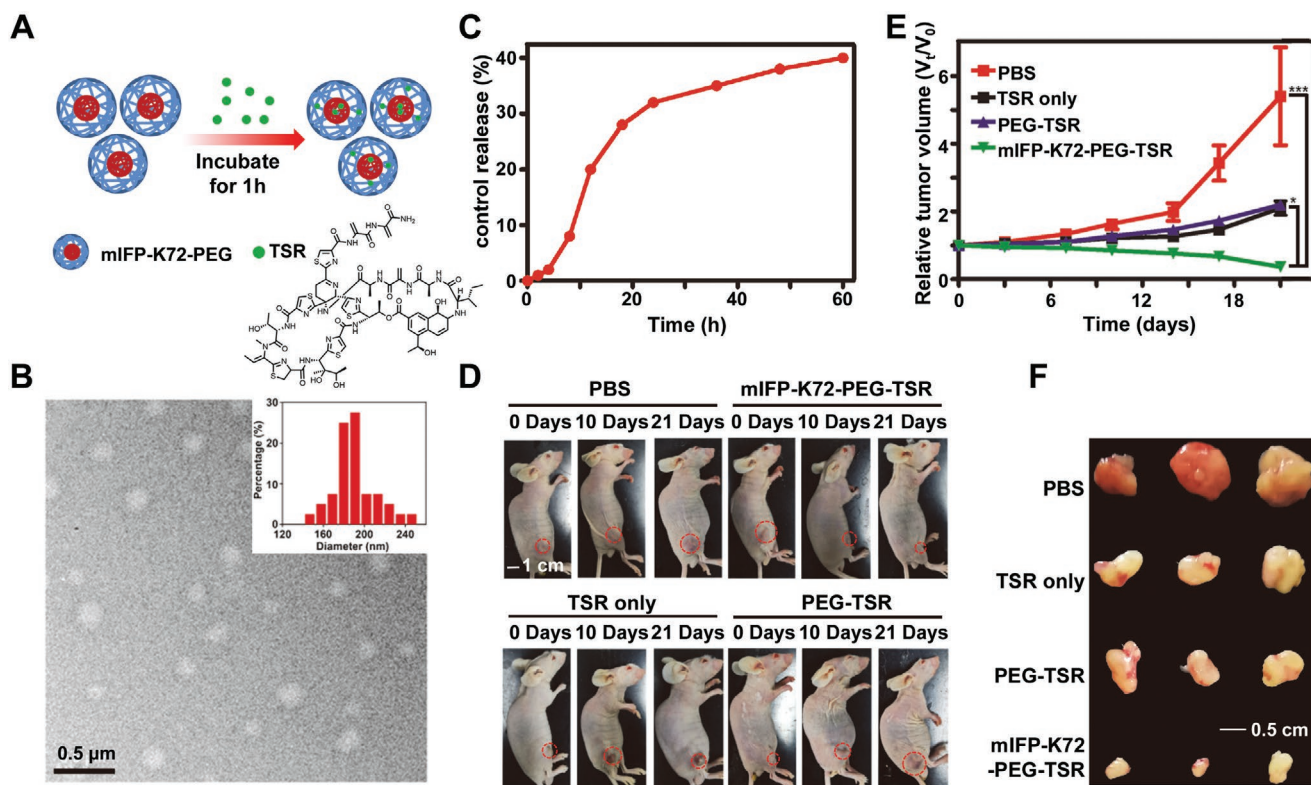


**Figure 4.** Investigation of antitumor effect of TSR-encapsulated mIFP-K72-PEG nanoparticles. A) Schematic of the TSR encapsulation within the mIFP-K72-PEG nanoparticles. B) TEM image and size distribution of the TSR-encapsulated mIFP-K72-PEG nanoparticles. The TSR-encapsulated mIFP-K72-PEG has a uniform structure with an average size of about 200 nm in diameter. Scale bar: 0.5  $\mu\text{m}$ . C) The release rate of TSR from mIFP-K72-PEG nanoparticles (characterized by a percentage of original dose). D) Photographs of the mice with tumor xenografts in the right hind leg after treatment with TSR-encapsulated mIFP-K72-PEG, pristine TSR, PEG-TSR, and PBS. Tumor sites are indicated by dashed red circles. Scale bar: 1 cm. E) Investigation of tumor volumes treated by each group ( $n = 5$ ,  $*p < 0.05$ ;  $***p < 0.001$ ). Tumors treated with TSR-encapsulated mIFP-K72-PEG nanoparticles were 6 $\times$  smaller in size than others. F) After the mice were sacrificed after 21 day treatment, all tumors were isolated and their size and morphology were captured. Scale bar: 0.5 cm.

of the mIFP-K72-PEG nanoparticles in the tumor area. Ex vivo imaging analysis was performed by harvesting the liver after 24 h post-injection (Figure 3C). In comparison with the mice treatment only with mIFP-K72-PEG (Figure 3C[e,d]) and PBS buffer (Figure 3C[e,f]), the mice injected with both MHCC97-H cells and mIFP-K72-PEG (Figure 3C[a,b]) exhibited fluorescence mainly in the liver. These results further suggest the feasibility of mIFP-K72-PEG for the detection of metastatic tumor nodules in vivo.

As the nanostructures of the mIFP-K72-PEG assembled in a well-defined manner, the drug loading and tumor therapy using these protein assemblies were evaluated by encapsulating the hydrophobic anticancer antibiotic thiostrepton (TSR) (Figure 4A).<sup>[39]</sup> It was found that  $\approx 36$  nmol of TSR were encapsulated in every nmol of the mIFP-K72-PEG complex (Figure S15, Supporting Information). A spherical structure of TSR-encapsulated nanoparticles (mIFP-K72-PEG-TSR) was observed by TEM (Figure 4B). There was no obvious difference in the sizes of nanoparticles before and after TSR encapsulation. This hinted toward the existence of free volume within mIFP-K72-PEG nanoparticles, which is useful for loading hydrophobic drugs, such as TSR. Moreover, it was found that nanoparticles assembled from short polypeptide chains, including K18 and K36, exhibited a lower encapsulation efficiency of TSR (Figure S15,

Supporting Information). Unlike PEGylation reactions through covalent binding between lysine or cysteine residues and PEG,<sup>[40]</sup> PEGylation via electrostatic interactions often is weakened in physiological environments due to ion presence and variable pH values, which allows for the release of anticancer drugs. Thus, in the present system, the release of TSR from its nanocarriers was examined by incubating mIFP-K72-PEG-TSR in PBS solutions at 37  $^{\circ}\text{C}$ . As shown in Figure 4C, more than 96% of TSR was retained in the nanocarriers within 10 h and 30% of the drug was released within 30 h. These results suggested the long-period maintenance of TSR encapsulation in the nanocarriers, which is required for sufficient drug accumulation in tumor sites and important for in vivo applications. In order to evaluate the effect of mIFP-K72-PEG-TSR on cancer cells, HeLa cells were used for the in vitro experiment. The results showed that treatment with  $800 \times 10^{-6}$  M of the mIFP-K72-PEG-TSR for 24 h led to about 95% apoptosis of HeLa cells (Figure S16, Supporting Information). MTT assays also confirmed the significant activity of mIFP-K72-PEG-TSR against HeLa cells (Figures S17 and S18, Supporting Information).

The in vivo effect of TSR-encapsulated nanoparticles on tumor treatment was subsequently tested in mice bearing HeLa cell xenografts. After establishing subcutaneous tumor xenografts, 60 nmol  $\text{kg}^{-1}$  of the mIFP-K72-PEG-TSR

nanoparticles and 2  $\mu\text{mol kg}^{-1}$  of pristine TSR were administered through mice tail vein, respectively. Another control group (PEG-TSR) was also treated with both 60  $\text{nmol kg}^{-1}$  of PEG-COO<sup>-</sup> and 2  $\mu\text{mol kg}^{-1}$  of TSR simultaneously. Tumor growth was then recorded after the drug treatment (Figure 4D; Figure S19, Supporting Information). It is clear that the group treated with mIFP-K72-PEG-TSR showed complete inhibition of tumor growth by up to 6 $\times$  when compared with the other three control groups (Figure 4E,F). Moreover, the group treated with PEG-TSR and pristine TSR had similar tumor sizes, indicating the used PEG chain had no anticancer effect. Those results clearly indicated the TSR encapsulation via mIFP-K72-PEG nanoparticles greatly enhanced the antitumor effect of TSR. This might be ascribed to the outstanding accumulation behavior of the mIFP-K72-PEG assemblies in tumor sites. Furthermore, the enhanced antitumor properties were also observed in the treatment of GFP-K72-PEG-TSR, suggesting the FPs had no side effect on the drug delivery process (Figure S20, Supporting Information).

In summary, we have developed a new type of NIR FPs nanoparticle by the assembly of positively charged mIFP conjugates and negatively charged PEG-COO<sup>-</sup> chains. The robust protein assemblies provide attractive features: 1) NIR excitation and emission within the phototherapeutic window; 2) high cell permeability; 3) negligible cytotoxicity and high biocompatibility; and 4) long-time and stable in vivo imaging by direct exogenous injection. Those characteristics are completely different from traditional imaging reagents, and overcome the limitations of FP bioimaging relying on gene transfection and fast fluorescence decay. Particularly, our strategy was successfully used for tracking subcutaneous tumor xenografts and deeply located metastatic tumor nodules in vivo. In addition, these types of protein assemblies were employed as a theranostic nanocarrier to encapsulate and deliver hydrophobic antitumor drugs effectively. Due to the deep penetrability, photostability, and biocompatibility of this class of protein nanomaterial, they offer a new opportunity for biomedical diagnosis and treatment. Furthermore, inspired by this strategy, various protein-based nanomaterials can be easily fabricated by genetically fusing other functional proteins for medical applications.

## Supporting Information

Supporting Information is available from the Wiley Online Library or from the author.

## Acknowledgements

J.L., B.L., and J.S. contributed equally to this work. This work was supported by the Scientific Instrument Developing Project of the Chinese Academy of Sciences (Grant No. ZDKYYQ20180001), the Jilin Province Science Fund for Excellent Young Scholars (20190103072JH), K. C. Wong Education Foundation (Grant No. GJTD-2018-09), the National Natural Science Foundation of China (Grant No. 21704099, 21877104, and 21834007), and National Key R&D Program of China (2018YFA0902600).

## Conflict of Interest

The authors declare no conflict of interest.

## Keywords

engineered proteins, nanoparticles, NIR fluorescent imaging, tumor therapy

Received: February 11, 2020

Revised: February 23, 2020

Published online: March 12, 2020

- [1] Y. Yang, Q. Zhao, W. Feng, F. Li, *Chem. Rev.* **2013**, *113*, 192.
- [2] J. Zhang, X. Chai, X. He, H. Kim, J. Yoon, H. Tian, *Chem. Soc. Rev.* **2019**, *48*, 683.
- [3] G. Hong, A. L. Antaris, H. Dai, *Nat. Biomed. Eng.* **2017**, *1*, 0010.
- [4] S. M. Fothergill, C. Joyce, F. Xie, *Nanoscale* **2018**, *10*, 20914.
- [5] C. Yao, W. Wang, P. Wang, M. Zhao, X. Li, F. Zhang, *Adv. Mater.* **2018**, *30*, 1704833.
- [6] B. Shi, N. Ren, L. Gu, G. Xu, R. Wang, T. Zhu, Y. Zhu, C. Fan, C. Zhao, H. Tian, *Angew. Chem., Int. Ed.* **2019**, *58*, 16826.
- [7] Z. Lei, C. Sun, P. Pei, S. Wang, D. Li, X. Zhang, F. Zhang, *Angew. Chem., Int. Ed.* **2019**, *58*, 8166.
- [8] A. Zebibula, N. Alifu, L. Xia, C. Sun, X. Yu, D. Xue, L. Liu, G. Li, J. Qian, *Adv. Funct. Mater.* **2018**, *28*, 1703451.
- [9] J. Cao, H. Zhu, D. Deng, B. Xue, L. Tang, D. Mahounga, Z. Qian, Y. Gu, *J. Biomed. Mater. Res., Part A* **2012**, *100A*, 958.
- [10] C. Li, W. Li, H. Liu, Y. Zhang, G. Chen, Z. Li, Q. Wang, *Angew. Chem., Int. Ed.* **2020**, *59*, 247.
- [11] S. Wilhelm, *ACS Nano* **2017**, *11*, 10644.
- [12] G. Chen, R. Jaskula-Sztul, C. R. Esquibel, I. Lou, Q. Zheng, A. Dammalapati, A. Harrison, K. W. Eliceiri, W. Tang, H. Chen, S. Gong, *Adv. Funct. Mater.* **2017**, *27*, 1604671.
- [13] M. Zhao, B. Li, P. Wang, L. Lu, Z. Zhang, L. Liu, S. Wang, D. Li, R. Wang, F. Zhang, *Adv. Mater.* **2018**, *30*, e1804982.
- [14] S. Zhu, R. Tian, A. L. Antaris, X. Chen, H. Dai, *Adv. Mater.* **2019**, *31*, 1900321.
- [15] E. L. Rosenthal, L. S. Moore, K. Tipirneni, E. de Boer, T. M. Stevens, Y. E. Hartman, W. R. Carroll, K. R. Zinn, J. M. Warram, *Clin. Cancer Res.* **2017**, *23*, 4744.
- [16] J. Wang, F. Lv, L. Liu, Y. Ma, S. Wang, *Coord. Chem. Rev.* **2018**, *354*, 135.
- [17] V. K. Sharma, T. J. McDonald, M. Sohn, G. A. K. Anquandah, M. Pettine, R. Zboril, *Chemosphere* **2017**, *188*, 403.
- [18] X. Zheng, Y. Tan, *Small* **2019**, 1903328.
- [19] A. Gnach, T. Lipinski, A. Bednarkiewicz, J. Rybka, J. A. Capobianco, *Chem. Soc. Rev.* **2015**, *44*, 1561.
- [20] Q. Jiang, S. Liu, J. Liu, Z. Wang, B. Ding, *Adv. Mater.* **2019**, *31*, 1804785.
- [21] E. L. Rosenthal, J. M. Warram, E. de Boer, T. K. Chung, M. L. Korb, M. Brandwein-Gensler, T. V. Strong, C. E. Schmalbach, A. B. Morlandt, G. Agarwal, Y. E. Hartman, W. R. Carroll, J. S. Richman, L. K. Clemons, L. M. Nabell, K. R. Zinn, *Clin. Cancer Res.* **2015**, *21*, 3658.
- [22] R. W. Gao, N. Teraphongphom, E. de Boer, N. S. van den Berg, V. Divi, M. J. Kaplan, N. J. Oberhelman, S. S. Hong, E. Capes, A. D. Colevas, J. M. Warram, E. L. Rosenthal, *Theranostics* **2018**, *8*, 2488.
- [23] R. N. Day, M. W. Davidson, *Chem. Soc. Rev.* **2009**, *38*, 2887.
- [24] R. Y. Tsieng, *Angew. Chem., Int. Ed.* **2009**, *48*, 5612.
- [25] R. Weissleder, V. Ntziachristos, *Nat. Med.* **2003**, *9*, 123.
- [26] T. Schroeder, *Nature* **2008**, *453*, 345.
- [27] R. Weissleder, M. J. Pittet, *Nature* **2008**, *452*, 580.
- [28] D. Yu, M. A. Baird, J. R. Allen, E. S. Howe, M. P. Klassen, A. Reade, K. Makhijani, Y. Song, S. Liu, Z. Murthy, S. Zhang, O. D. Weiner,

- T. B. Kornberg, Y. Jan, M. W. Davidson, X. Shu, *Nat. Methods* **2015**, *12*, 763.
- [29] W. Lin, S. Mehta, J. Zhang, *J. Biol. Chem.* **2019**, *294*, 14814.
- [30] T. To, B. J. Piggott, K. Makhijani, D. Yu, Y. N. Jan, X. Shu, *Proc. Natl. Acad. Sci. USA* **2015**, *112*, 3338.
- [31] R. M. Hoffman, *Lancet Oncol.* **2002**, *3*, 546.
- [32] M. Yang, E. Baranov, P. Jiang, F.-X. Sun, X.-M. Li, L. Li, S. Hasegawa, M. Bouvet, M. Al-Tuwaijri, T. Chishima, H. Shimada, A. R. Moossa, S. Penman, R. M. Hoffman, *Proc. Natl. Acad. Sci. USA* **2000**, *97*, 1206.
- [33] C. Ma, A. Malessa, A. J. Boersma, K. Liu, A. Herrmann, *Adv. Mater.*, <https://doi.org/10.1002/adma.201905309>.
- [34] D. Bojar, M. Fussenegger, *Small*, <https://doi.org/10.1002/smll.201903093>.
- [35] J. Fang, H. Nakamura, H. Maeda, *Adv. Drug Delivery Rev.* **2011**, *63*, 136.
- [36] H. Maeda, H. Nakamura, J. Fang, *Adv. Drug Delivery Rev.* **2013**, *65*, 71.
- [37] D. Yu, W. C. Gustafson, C. Han, C. Lafaye, M. Noirclerc-Savoie, W. P. Ge, D. A. Thayer, H. Huang, T. B. Kornberg, A. Royant, L. Y. Jan, Y. N. Jan, W. A. Weiss, X. Shu, *Nat. Commun.* **2014**, *5*, 3626.
- [38] Y. Wu, C. Li, F. Boldt, Y. Wang, S. L. Kuan, T. T. Tran, V. Mikhalevich, C. Förtsch, H. Barth, Z. Yang, D. Liu, T. Weil, *Chem. Commun.* **2014**, *50*, 14620.
- [39] J. Wang, Z. Lin, X. Bai, J. Tao, W. Liu, *Org. Chem. Front.* **2019**, *6*, 1194.
- [40] M. J. Roberts, M. D. Bentley, J. M. Harris, *Adv. Drug Delivery Rev.* **2012**, *64*, 116.